Optimization of Raman Amplification in Silicon Waveguides With Finite Facet Reflectivities

Ivan D. Rukhlenko, Chethiya Dissanayake, Malin Premaratne, *Senior Member, IEEE*, and Govind P. Agrawal, *Fellow, IEEE*

***Abstract*—Increasing the amplifying efficiency in silicon-on-insulator waveguides plays a crucial role in future adaptation of this technology for integrated optics applications. Such improvements not only lead to a reduced overall footprint size but also the overall reduction in the operating energy consumption of the device. In this paper, we address the design optimization of silicon optical amplifiers working in the continuous wave domain. We seek to optimize the efficiency of a silicon optical amplifier by varying the cross-section area along the waveguide length that coerces judicious minimization of the pernicious influence of free-carrier absorption and two-photon absorption on Raman amplification. Using a recently proposed semi-analytical technique, we recasted the above problem as a boundary-value problem that contains eight coupled nonlinear differential equations for four waves' powers and four auxiliary functions. The numerical solution of these equations allows one to find the axial profile of the effective mode area (EMA), providing the largest output signal power for given waveguide length, input pump power and a preset, input-facet EMA. We have illustrated utility of our method by applying it to several practically realizable amplification scenarios. In particular, optimizing the EMA profiles with different input-facet EMAs, we calculated the optimum signal gain of a silicon optical amplifier with a given (i.e., preset) amplifier length.**

***Index Terms*—Integrated optics, nonlinear optics, Raman effect, silicon photonics, silicon Raman amplifiers, silicon waveguides, waveguide tapering.**

I. Introduction

THE UNIQUE nonlinear optical properties of silicon provide a large number of promising applications for silicon-on-insulator (SOI) waveguides (also called photonic nanowires) in optoelectronic-integrated circuits [1]–[4]. These properties owe their existence to the pronounced Kerr effect, stimulated Raman scattering (SRS), two-photon absorption (TPA), and free-carrier absorption (FCA), which are intrinsic to the crystalline silicon within the 1.55-μm telecommunications window [4]–[6]. Among a plethora of silicon-based device functionalities that have been demonstrated during the last decade, the Raman amplification in SOI waveguides is one of the most versatile and remarkable effect making this technology attractive for practical applications [7]–[9].

It is well known that the Raman gain coefficient for SRS is about four orders of magnitude higher in silicon than that for fused silica [5], [10], [11]. This feature made it possible for several experimental groups to demonstrate a net positive gain for both pulsed [8], [12]–[16] and continuous-wave (CW) [17], [18] silicon Raman amplifiers. However, the operating intensity levels of such amplifiers are severely limited by the free carriers generated via the TPA mechanism. This happens because TPA-generated carriers give rise to strong FCA, which is cumulative in nature and grows as square of the optical intensity. Thus, FCA is the main detrimental effect that hinders a net positive Raman gain in silicon and directly affects the performance of Raman amplifiers [19]–[22].

In the case of CW-pumped Raman amplifiers, the problem of FCA is tackled by removing the free carriers from the modal area using a reverse-biased p-n junction [22]–[25]. In amplifiers operating in the pulsed regime, the negative impact of FCA can also be alleviated by reducing the pulse repetition rate [15] (such that most of carriers generated by one pulse vanish through recombination before the next pulse arrives) or by making the width of pump pulses narrower than the effective carrier lifetime [12]. Even after implementing these very effective remedies, there still remains scope to further improve the performance of CW Raman amplifiers by tapering the waveguide appropriately [26]–[29]. One can easily understand the physics behind this strategy by noting that the efficiency of SRS is proportional to the first power of intensity and thus changes slower than that of FCA. As a result, by varying the cross-section area of a silicon waveguide, one may attain a balance between Raman amplification, TPA, and FCA, and thus achieve maximum signal gain for a given carrier lifetime, waveguide length, and input powers.

We, recently, proposed a semi-analytical method that allows one to find the optimal axial profile of the effective mode area (EMA) along the length of a single-pass Raman amplifier [29]. It was shown there that the gain optimization can be performed by solving a boundary-value problem associated with pump and signal powers that are linked to each other through some judiciously introduced auxiliary functions. However, reflections from the input and output facets of the SOI waveguide were ignored to avoid backward propagation of the pump and signal waves. In the present paper, we extend this method to a more realistic scenario where backward-propagating pump and signal waves exist within the amplifier because of finite facet reflectivities at the waveguide ends. We show that, in this case, a set

Manuscript received April 22, 2009; revised August 7, 2009. First published October 6, 2009; current version published February 5, 2010. This work was supported by the Australian Research Council through its Discovery Grant Scheme under Grant DP0877232. The work of G. P. Agrawal was also supported by the National Science Foundation Award ECCS-0801772.

I. D. Rukhlenko, C. Dissanayake, and M. Premaratne are with the Advanced Computing and Simulation Laboratory, Department of Electrical and Computer Systems Engineering, Monash University, Clayton, Vic. 3800, Australia (e-mail: ivan.rukhlenko@eng.monash.edu.au; chethiya.dissanayake@eng.monash.edu.au; malin@eng.monash.edu.au).

G. P. Agrawal is with the Institute of Optics, University of Rochester, Rochester, NY 14627-0186 USA (e-mail: gpa@optics.rochester.edu).

Digital Object Identifier 10.1109/JSTQE.2009.2030512

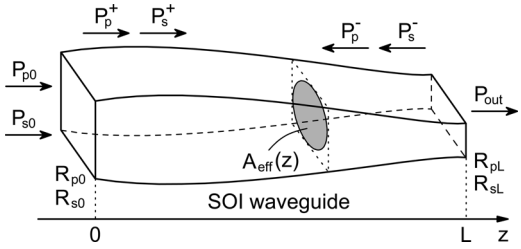

Fig. 1. Scheme of the SOI waveguide with variable cross section and the propagating waves considered in this paper. The input pump and signal powers are denoted by P_{p0} and P_{s0}, respectively; R_{p0}, R_{s0}, R_{pL}, and R_{sL} are the reflectivities for pump and signal wavelengths at the input ($z = 0$) and output ($z = L$) ends of the waveguide; $P_{\rm out}$ is the output signal power. The effective mode area, $A_{\rm eff}\,(z)$, is proportional to the waveguide cross-section area shown by dotted lines.

of eight nonlinear differential equations need to be solved to obtain the optimal EMA profile. Within the validity region of undepleted pump approximation, the solution of these equations reduces to the well-known analytical result of Renner *et al.* [26]. We further illustrate the effectiveness of our method by considering the depleted-pump scenario and discuss the possibility of linear tapering instead of optimized tapering.

II. Optimization Procedure

Consider the process of Raman amplification of a CW signal at the Stokes frequency $\omega_s = 2\pi c/\lambda_s$ by a CW pump at frequency $\omega_p = 2\pi c/\lambda_p$ inside the SOI waveguide of variable cross section (see Fig. 1). Owing to the nonzero reflectivities at facets of the waveguide, both forward (+) and backward (−) propagating waves coexist within the amplifier. The evolution of the powers associated with these four waves, $P_p^{\pm}(z)$ and $P_s^{\pm}(z)$, inside the waveguide is governed by the following set of coupled differential equations used frequently for modeling silicon Raman lasers [26], [27], [30]:

$$\pm\frac{1}{P_p^{\pm}}\frac{dP_p^{\pm}}{dz} = -\alpha-\beta\frac{P_p^{\pm}+2P_p^{\mp}}{A_{\rm eff}} - \zeta_{ps}\frac{P_s^{+}+P_s^{-}}{A_{\rm eff}} - \kappa_p\frac{\mathcal{P}^2}{A_{\rm eff}^2}, \quad (1a)$$

$$\pm\frac{1}{P_s^{\pm}}\frac{dP_s^{\pm}}{dz} = -\alpha-\beta\frac{P_s^{\pm}+2P_s^{\mp}}{A_{\rm eff}} - \zeta_{sp}\frac{P_p^{+}+P_p^{-}}{A_{\rm eff}} - \kappa_s\frac{\mathcal{P}^2}{A_{\rm eff}^2}. \quad (1b)$$

Here α and β are, respectively, the linear loss and TPA coefficients, assumed to be equal at the pump and Stokes frequencies, $A_{\rm eff}\,(z)$ is the z-dependent EMA of the waveguide mode excited by the pump and signal waves, and $\mathcal{P}^2$ accounts for different channels through which free carriers are generated inside the waveguide,

$$\mathcal{P}^2 = (P_p^{+})^2+(P_p^{-})^2+(P_s^{+})^2+(P_s^{-})^2 + 4\big[P_p^{+}P_p^{-}+P_s^{+}P_s^{-}+(P_p^{+}+P_p^{-})(P_s^{+}+P_s^{-})\big].$$

The FCA is included in (1) through the last term and is determined by the coefficients $\kappa_{p(s)} = \tau_c\sigma_{p(s)}\beta/(2\hbar\omega_p)$, where τ_c is the effective carrier lifetime, $\sigma_{p(s)} = \sigma_0(\lambda_{p(s)}/\lambda_0)^2$, $\sigma_0 = 1.45\times10^{-21}\,{\rm m}^2$, and $\lambda_0 = 1550$ nm. The coefficients

$$\zeta_{ps} = 2\beta + g_R\mathcal{L}(\Omega_{ps}) \ \text{ and } \ \zeta_{sp} = (\omega_s/\omega_p)[2\beta - g_R\mathcal{L}(\Omega_{ps})]$$

are responsible for cross-TPA through the β-term and for SRS through the Raman gain coefficient g_R. The Lorentzian function

$$\mathcal{L}(\Omega_{ps}) = \frac{4\gamma_R^2\Omega_R\Omega_{ps}}{(\Omega_R^2-\Omega_{ps}^2)^2+4\gamma_R^2\Omega_{ps}^2}$$

takes into account the shape of the Raman-gain spectrum. Here $\Omega_{ps} = \omega_p - \omega_s$, $\Omega_R = 15.6$ THz is the Stokes shift, and $\gamma_R = 105$ GHz is the Raman-gain bandwidth at room temperature. It is significant that $\beta \ll g_R$ in silicon. Therefore, near the Raman-gain peak ($\Omega_{ps}\approx\Omega_R$), $\zeta_{sp} < 0$, and the third term in the right-hand side of (1b) is positive.

The boundary conditions for powers entering system (1) are determined by the reflectivities, $R_{p(s)0}$ and $R_{p(s)L}$, for the pump and signal at the input and output ends of the waveguide as well as by the input powers, P_{p0} and P_{s0}, launched into the waveguide (see Fig. 1). In particular, R_{p0} and R_{s0} determine what fraction of the input powers is reflected from the waveguide and not involved in the amplification process. It is easy to see that the forward- and backward-propagating waves at the two waveguide ends are related by the following boundary conditions:

$$P_p^{+}(0) = (1-R_{p0})P_{p0} + R_{p0}P_p^{-}(0), \quad (2a)$$

$$P_s^{+}(0) = (1-R_{s0})P_{s0} + R_{s0}P_s^{-}(0), \quad (2b)$$

$$P_p^{-}(L) = R_{pL}P_p^{+}(L), \quad (2c)$$

$$P_s^{-}(L) = R_{sL}P_s^{+}(L). \quad (2d)$$

Notice that, in the case $R_{p0} = R_{s0} = R_{pL} = R_{sL} = 0$, the boundary-value problem given by (1) and (2) describes a single-pass Raman amplifier, whereas the case $P_{s0} = 0$ corresponds to the Raman laser. Thus, our general analysis covers these two important devices as special cases.

It follows from (1) that the signal gain depends drastically on the EMA profile. If the waveguide has a very large area all along its length, the nonlinear terms in (1b) are negligible, and the signal experiences only the linear absorption. By contrast, in a very small cross-section waveguide, strong nonlinear absorption occurs, and Raman amplification becomes quite inefficient. Therefore, one can reasonably expect to find an optimal EMA profile that maximizes the output signal power

$$P_{\rm out} \equiv P_s^{+}(L) - P_s^{-}(L) = (1-R_{sL})P_s^{+}(L). \quad (3)$$

Such a profile indeed exists. We now show that it can be found by employing the method proposed earlier for maximization of the net optical gain in single-pass silicon Raman amplifiers [29]. Since EMA is proportional to the amplifier cross-section area, it can be altered in practice by tapering the waveguide width or thickness (or both) appropriately.

According to the variations calculus [31], the optimal EMA profile, $A_{\rm eff}\,(z)$, makes the output signal power stationary with respect to small variations $\delta A_{\rm eff}\,(z)$. Mathematically, the first

variation of $P_{\rm out}$ should vanish, i.e., $\delta P_{\rm out} = 0$, or, what is the same through relation (3)

$$\delta P_s^+(L) = 0.$$

We provide details of the mathematical process that we use to satisfy this condition in the Appendix. Utilizing (A2b) and (2d), it is straightforward to show that the preceding equation can be represented in the form

$$\delta G_s^+ = R_{s0}\,\frac{P_s^-(0)}{P_s^+(0)}\,\delta G_s^-, \tag{4}$$

where $G_s^\pm$ represents the net Raman amplification (on a log scale) of the signal in the forward and backward directions,

$$G_s^\pm = \ln\frac{P_s^\pm(L)}{P_s^\pm(0)} = \int_0^L \frac{1}{P_s^\pm}\frac{dP_s^\pm}{dz}\,dz$$

assuming that $P_{s0} \neq 0$ and $R_{s0} \neq 1$. At this point, it should be emphasized that the present optimization problem is significantly more difficult than that for a single-pass silicon Raman amplifier because (4) contains unknown functions at the waveguide input end.

Using (1b), we can rewrite (4) as an integral equation containing small variations of pump and signal powers corresponding to $\delta A_{\rm eff}(z)$. The optimal EMA profile can be expressed from this equation by introducing four auxiliary functions and employing the integro-variational consequences of the propagation equations (1) as well as variational consequences of the boundary conditions (2) in the same manner as was done in [29]. The details are given in the Appendix and lead to the following final result:

$$A_{\rm eff}(z) = \frac{N_{ps}(z)}{D_{ps}(z)}, \tag{5}$$

where

$$\begin{aligned}
N_{ps}(z) &= 2\mathcal{P}^2[\kappa_s(1+\vartheta-\psi_+P_s^+ + \psi_-P_s^-)\\
&\quad - \kappa_p(\varphi_+P_p^+ - \varphi_-P_p^-)],\\
D_{ps}(z) &= \varphi_+P_p^+[\beta(P_p^+ + 2P_p^-) + \zeta_{ps}(P_s^+ + P_s^-)]\\
&\quad - \varphi_-P_p^-[\beta(P_p^- + 2P_p^+) + \zeta_{ps}(P_s^+ + P_s^-)]\\
&\quad + \psi_+P_s^+[\beta(P_s^+ + 2P_s^-) + \zeta_{sp}(P_p^+ + P_p^-)]\\
&\quad - \psi_-P_s^-[\beta(P_s^- + 2P_s^+) + \zeta_{sp}(P_p^+ + P_p^-)]\\
&\quad - \beta[(1+2\vartheta)P_s^+ + (2+\vartheta)P_s^-]\\
&\quad - \zeta_{sp}(1+\vartheta)(P_p^+ + P_p^-),
\end{aligned}$$

and $\vartheta = R_{s0}P_s^-(0)/P_s^+(0)$.

The auxiliary functions $\varphi_\pm$ and $\psi_\pm$ satisfy four coupled nonlinear differential equations,

$$\frac{d\varphi_\pm}{dz} = a_p^\pm\varphi_+ - \widetilde{a}_p^\pm\varphi_- + b_p^\pm\psi_+ - \widetilde{b}_p^\pm\psi_- - \mathcal{A}^\pm, \tag{6a}$$

$$\frac{d\psi_\pm}{dz} = a_s^\pm\psi_+ - \widetilde{a}_s^\pm\psi_- + b_s^\pm\varphi_+ - \widetilde{b}_s^\pm\varphi_- - \mathcal{B}^\pm, \tag{6b}$$

that should be solved with the boundary conditions

$$\varphi_+(L) = -R_{pL}\varphi_-(L), \tag{7a}$$

$$\varphi_-(0) = -R_{p0}\varphi_+(0), \tag{7b}$$

$$\psi_-(0) = -R_{s0}\psi_+(0). \tag{7c}$$

The fourth boundary condition involves the EMA at the input (or output) end of the waveguide, i.e.,

$$A_{\rm eff}(0) = A_0 \ [\text{or } A_{\rm eff}(L) = A_L]. \tag{8}$$

All coefficients appearing in (6) vary with z and are given by

$$\begin{aligned}
\mathcal{A}^\pm &= \frac{1+\vartheta}{A_{\rm eff}}\left[\zeta_{sp} + 2\kappa_s\,\frac{P_p^\pm + 2(P_p^\mp + P_s^+ + P_s^-)}{A_{\rm eff}}\right],\\
\mathcal{B}^\pm &= \frac{1}{A_{\rm eff}}\left[2^{1/2}(2^{\mp 1/2} + 2^{\pm 1/2}\vartheta)\beta\right.\\
&\qquad \left. + 2(1+\vartheta)\kappa_s\,\frac{P_s^+ + 2(P_s^- + P_p^+ + P_p^-)}{A_{\rm eff}}\right],\\
a_p^+ &= \alpha + 2\beta\,\frac{P_p^+ + P_p^-}{A_{\rm eff}} + \zeta_{ps}\frac{P_s^+ + P_s^-}{A_{\rm eff}}\\
&\quad + \kappa_p\,\frac{\mathcal{P}^2 + 2P_p^+[P_p^+ + 2(P_p^- + P_s^+ + P_s^-)]}{A_{\rm eff}^2},\\
a_p^- &= 2\,\frac{P_p^+}{A_{\rm eff}}\left[\beta + \kappa_p\,\frac{P_p^- + 2(P_p^+ + P_s^+ + P_s^-)}{A_{\rm eff}}\right].
\end{aligned}$$

The coefficients $a_s^\pm$ are obtained from $a_p^\pm$ by interchanging the subscripts p and s, whereas the coefficients $\widetilde{a}_{p(s)}^\pm$ are obtained from $a_{p(s)}^\mp$ by interchanging the superscripts "+" and "−". Finally, $b_s^\pm$ and $\widetilde{b}_s^\pm$ are obtained, respectively, using $b_p^\pm = \mathcal{A}^\pm P_s^+/(1+\vartheta)$ and $\widetilde{b}_p^\pm = (P_s^-/P_s^+)\,b_p^\pm$.

Thus, the procedure for finding the EMA profile consists of solving a set of eight equations in (1) and (6) subject to the boundary conditions in (2), (7), and (8). The optimum EMA profile $A_{\rm eff}(z)$ is then found from (5). Following the same arguments as in the case of a single-pass Raman amplifier [29], it can be proved that this choice leads to the maximal value for the amplified signal power $P_{\rm out}$ in (3). We note that, if all reflectivities were zero, the backward-propagating waves are absent and $\vartheta = 0$. In this case, (1), (5), and (6) reduce to those derived earlier in [29] for a single-pass Raman amplifier.

At the end of this section, it should be emphasized that the above gain optimization scheme is only applicable to the idealized situation where both the pump and the signal are continuous waves. In real silicon Raman amplifiers, finite bandwidths of interacting waves and the limited bandwidth of the Raman response result in the signal receiving uneven gain across its spectral profile. The problem of simultaneous gain maximization and gain profile flattening is more complicated and requires full-blown numerical simulations. The study of this interesting problem is now in progress.

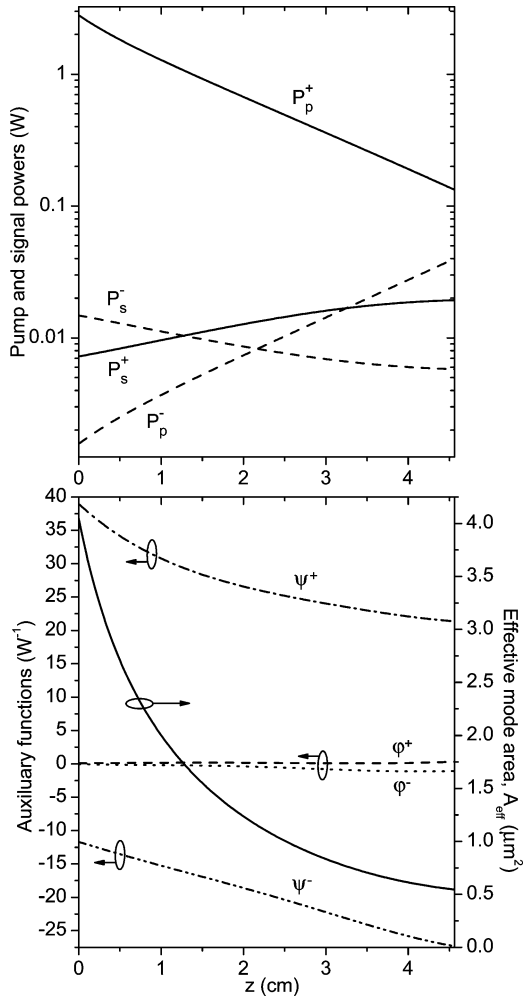

Fig. 2. Evolution of powers for the forward-(solid curves) and backward-(dashed curves) propagating pump and signal when input pump power is so large that the undepleted-pump approximation is valid (upper panel). Four auxiliary functions (broken curves, left scale) and the optimized EMA axial profile (solid curve, right scale) (lower panel). The reflectivities at pump and signal wavelength are assumed to be equal to 0.3 at both facets of the waveguide. The simulation parameters are: $L = 45.6$ mm, $P_{p0} = 4$ W, $P_{s0} = 0.004$ W, and $A_0 = 4\,\mu\mathrm{m}^2$. For other parameters see the text.

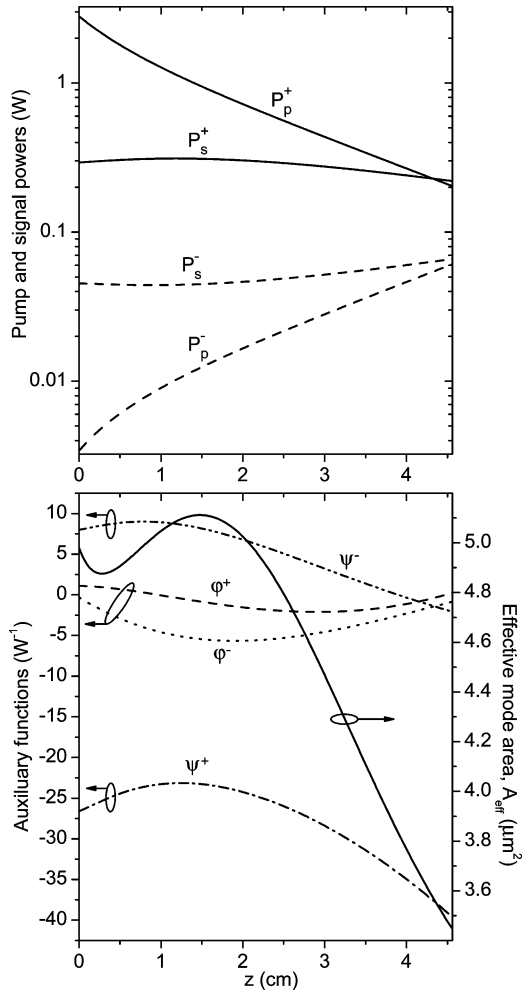

Fig. 3. Solution of coupled equations in (1) and (6) when $P_{p0} = 4$ W, $P_{s0} = 0.4$ W, and $A_0 = 5\ \mu\mathrm{m}^2$. Powers of forward-(solid curves) and backward-(dashed curves) traveling waves as functions of propagation distance (upper panel). Optimized EMA profile (solid curve, right scale) and the auxiliary functions (broken curves, left scale) (lower panel). All other parameters are the same as employed in Fig. 2.

III. Numerical Results and Discussion

As an example, we consider in this section the optimization problem when a 1542-nm CW signal is amplified through SRS by a 1427-nm pump inside a silicon waveguide of fixed length $L = 45.6$ mm. In our numerical simulations, we employ the following typical parameter values for a silicon waveguide: $R_{p0} = R_{s0} = R_{pL} = R_{sL} = 0.3$, $\alpha = 1$ dB/cm, $\beta = 0.7$ cm/GW, $g_R = 20$ cm/GW, and $\tau_c = 4.5$ ns.

Let us start by examining the special situation in which the depletion of forward-propagating pump is negligibly small. As is well-known [26], the optimal tapering profile in this case has a simple exponential shape along the amplifier length. The undepleted-pump scenario is realized numerically, for example, when a 4-mW signal and a 4-W pump are launched inside the SOI waveguide with $A_0 = 4\,\mu\mathrm{m}^2$. The solution of the boundary-value problem specified by (1), (2), (6)–(8) in this case, is presented in Fig. 2. The upper panel shows the four power levels, $P_p^{\pm}$ and $P_s^{\pm}$, while the lower panel shows the four auxiliary functions, $\varphi_{\pm}$ and $\psi_{\pm}$. The optimum EMA profile calculated by using (5) is shown by the solid curve in the lower panel. It is readily seen that EMA decreases exponentially towards the waveguide output, in agreement with the prediction of [26].

The consistency of our method with the prediction of [26] can also be proved analytically. To do this, we notice that, in the undepleted pump approximation, $P_p^+ \gg P_p^-, P_s^{\pm}$ and $\varphi_{\pm} \to 0$. As a consequence, all the terms proportional to these small quantities can be omitted in (5), and we recover the analytic result

$$A_{\mathrm{eff}}(z) = \frac{2\kappa_s}{|\zeta_{sp}|}\, P_p^+(z) = A_0 \exp(-qz),$$

where $A_0 = 2\kappa_s P_{p0}/|\zeta_{sp}|$ and $q = \alpha + \beta P_{p0}/A_0 + \kappa_p (P_{p0}/A_0)^2$. In this case, the exponential dependence of $P_p^+(z)$ on z follows from (1a) after noting that $P_p^+(z) \propto A_{\mathrm{eff}}(z)$.

The more interesting case is the one in which pump depletion cannot be ignored. Fig. 3 shows the numerical results

in this case using incident powers $P_{p0} = 4$ W and $P_{s0} = 0.4$ W. The upper and lower panels show again the evolution of pump and signal powers and the four auxiliary functions. The corresponding optimum EMA profile is shown by the solid curve in the lower panel. In contrast to the undepleted-pump case, the optimized EMA profile is no longer a monotonous function of the distance from the input facet. Instead, it first decreases, increases between $z = 0.4$ and 1.5 cm, and then decreases again. The EMA increase in the middle reduces the nonlinear interactions governed by the last three terms in (1), and thus conserves pump's energy for the second half of the waveguide. The result is that the net power transfer from the pump exchange to the signal is enhanced.

The EMA profile, shown in Fig. 3, depends critically on the initial EMA, A_0, at the input end of the waveguide. This dependence is shown in the upper panel of Fig. 4 under the same operating conditions as those used in Fig. 3. In particular, we choose $P_{p0} = 4$ W and $P_{s0} = 0.4$ W. When the input EMA, A_0, is relatively small and the input intensities are high, pump depletion plays an important role, and the EMA profile has an irregular shape. However, for large values of the A_0, the Raman interaction becomes relatively weak, and the EMA profile tends to exponentially decrease along the waveguide. Clearly, there is only one amplifier that will provide the largest $P_{\rm out}$ for given waveguide length and input powers. The initial EMA of this amplifier can be found from the lower panel of Fig. 4. In this panel, solid curve shows the dependence of output signal power on the initial EMA for $P_{p0} = 4$ W and $P_{s0} = 0.4$ W. One can see that the absolute maximal output signal power of $P_{\max} \approx 174$ mW is realized inside an EMA-optimized waveguide with $A_0 \approx 10\ \mu\mathrm{m}^2$. For comparison, in the same panel we show the corresponding behavior for untapered waveguides (dotted curve) and for waveguides optimized by employing linear tapering (dashed curve). The solid vertical line shows the point where the case of linear tapering concurs with a waveguide of constant EMA $A_{\rm c} \approx 5.9\ \mu\mathrm{m}^2$.

The physics behind linear tapering can be easily understood. In the case of $A_0 < A_{\rm c}$, the TPA and FCA phenomena dominate over the SRS near the input end of the Raman amplifier but an expansion of the waveguide reduces the impact of FCA and increases the signal gain. The situation is different when $A_0 > A_{\rm c}$. In this case, the nonlinear processes are weak at the input end, and a narrowing of the waveguide is needed to increase the efficiency of SRS and $P_{\rm out}$. It should be noted that, for $A_0 < A_{\rm c}$, silicon waveguides with constant EMAs all along their lengths provide almost the same signal gain as optimized linear-tapered waveguides. The difference between signal gains in these two types of the waveguides becomes considerable only if $A_0 > A_{\rm c}$.

The proximity of the solid and dashed curves in the lower panel of Fig. 4 allows one to conclude that, for each optimized amplifier, there exist a linearly-tapered waveguide that gives nearly the same signal gain. Thus, similar to the case of a single-pass amplifier, we can formulate the following practically important design rule for silicon Raman amplifiers. Instead of reproducing the optimal EMA profile, which typically has an irregular shape, it may be more practical to look for an optimal linear tapering profile of the amplifier. Even though the output signal power is somewhat reduced in the later case, the fabrication of a linearly-tapered waveguide is often much simpler in practice.

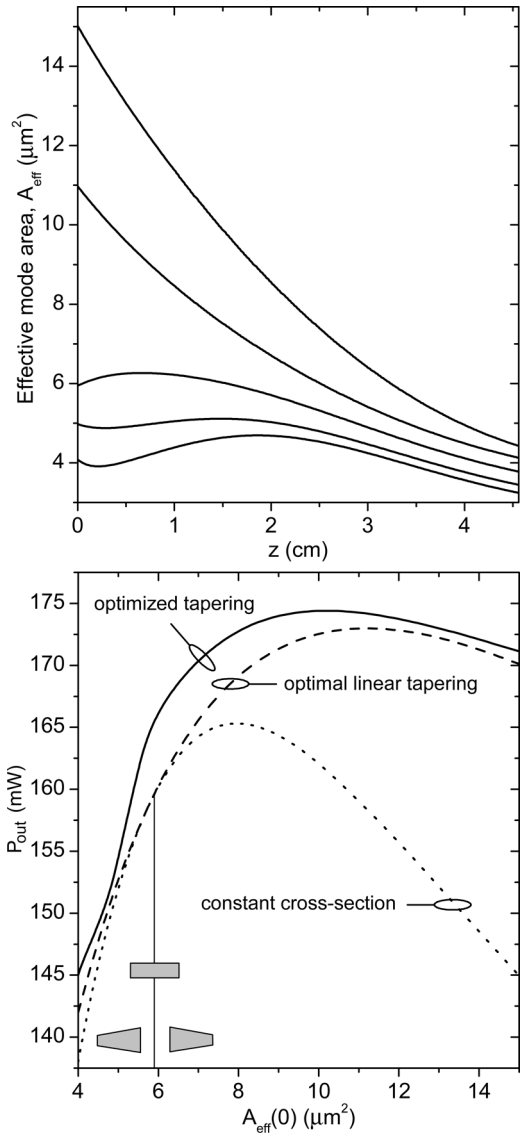

Fig. 4. Optimized EMA profiles for different values of $A_{\rm eff}(0)$ under operating conditions identical to those used for Fig. 3 (upper panel). Output signal powers in EMA-optimized waveguides (solid curve), optimized linear-tapered waveguides (dashed curve), and constant-EMA waveguides (dotted curve) for different input EMAs (lower panel). The vertical line shows the location where dashed and dotted curves coincide. The shaded quadrangles represent schematically the longitudinal profile of a waveguide assuming that its input is on the left.

IV. Conclusion

A new numerical algorithm for optimizing the axial EMA profile of continuously-pumped silicon Raman amplifiers has been developed in the most general case in which the reflections at the end facets of the SOI waveguide are not negligible. Such reflections lead to the simultaneous existence of both the forward- and backward-propagating signal and pump waves within the amplifier. Surpassing our previous paper in this area, we account for all these waves and reformulate the optimization problem

as a variational problem with several auxiliary functions. The method, we used, is very instructive in the sense that it shows an application of modern variational analysis to design silicon Raman amplifiers that provides maximum signal amplification at a given pump power by solving the underlying nonlinear propagation problem. The implementation of the algorithm requires the numerical solution of a boundary-value problem involving eight first-order coupled differential equations, but it allows one to find the optimum EMA profile along the waveguide length. This profile balances the effects of nonlinear absorption (TPA and FCA) and Raman amplification inside the silicon waveguide such that the output signal power attains its maximum possible value. Since the EMA is proportional to the waveguide cross-section area, the optimum EMA profile can be realized in practice by tapering the waveguide along its length appropriately. Numerical examples have revealed that the optimized linear tapering of the waveguide is able to provide almost the same output signal power as the optimal tapering with an irregular shape. This peculiarity can be used to substantially simplify the fabrication of practical optimized devices.

APPENDIX

DETAILS OF THE VARIATIONAL PROCEDURE

To show that the condition (4) leads to the EMA profile given in (5), provided that (6) and (7) are satisfied, we rewrite (4) using (1b) in the form

$$\int_0^L \frac{\mathcal{A}^+\delta P_p^+ + \mathcal{A}^-\delta P_p^- + \mathcal{B}^+\delta P_s^+ + \mathcal{B}^-\delta P_s^-}{A_{\rm eff}}\,dz = \int_0^L \delta A_{\rm eff}\left[\frac{\beta(1+2\vartheta)P_s^+ + \beta(2+\vartheta)P_s^-}{A_{\rm eff}^2} + \frac{\zeta_{sp}(1+\vartheta)(P_p^+ + P_p^-)}{A_{\rm eff}^2} + \frac{2(1+\vartheta)\kappa_s\mathcal{P}^2}{A_{\rm eff}^3}\right]dz. \quad \text{(A1)}$$

Taking the variations of (1a) and (1b), multiplying the resulting equations by auxiliary functions $\varphi_+(z)$, $\varphi_-(z)$, $\psi_+(z)$, and $\psi_-(z)$, and integrating them with respect to z from 0 to L, we obtain the following four equations:

$$\varphi_+(L)\delta P_p^+(L) - \varphi_+(0)\delta P_p^+(0) - \int_0^L \frac{d\varphi_+}{dz}\,\delta P_p^+\,dz = -\int_0^L \varphi_+(a_p^+\delta P_p^+ + a_p^-\delta P_p^- + b_s^+\delta P_s^+ + b_s^-\delta P_s^-)\,dz + \int_0^L \frac{\varphi_+ P_p^+ Q_{ps}}{A_{\rm eff}^2}\,\delta A_{\rm eff}\,dz,$$

$$\varphi_-(L)\delta P_p^-(L) - \varphi_-(0)\delta P_p^-(0) - \int_0^L \frac{d\varphi_-}{dz}\,\delta P_p^-\,dz = \int_0^L \varphi_-(\widetilde{a}_p^+\delta P_p^+ + \widetilde{a}_p^-\delta P_p^- + \widetilde{b}_s^+\delta P_s^+ + \widetilde{b}_s^-\delta P_s^-)\,dz - \int_0^L \frac{\varphi_- P_p^- Q_{ps}}{A_{\rm eff}^2}\,\delta A_{\rm eff}\,dz,$$

$$\psi_+(L)\delta P_s^+(L) - \psi_+(0)\delta P_s^+(0) - \int_0^L \frac{d\psi_+}{dz}\,\delta P_s^+\,dz = -\int_0^L \psi_+(b_p^+\delta P_p^+ + b_p^-\delta P_p^- + a_s^+\delta P_s^+ + a_s^-\delta P_s^-)\,dz + \int_0^L \frac{\psi_+ P_s^+ Q_{sp}}{A_{\rm eff}^2}\,\delta A_{\rm eff}\,dz,$$

$$\psi_-(L)\delta P_s^-(L) - \psi_-(0)\delta P_s^-(0) - \int_0^L \frac{d\psi_-}{dz}\,\delta P_s^-\,dz = \int_0^L \psi_-(\widetilde{b}_p^+\delta P_p^+ + \widetilde{b}_p^-\delta P_p^- + \widetilde{a}_s^+\delta P_s^+ + \widetilde{a}_s^-\delta P_s^-)\,dz - \int_0^L \frac{\psi_- P_s^- Q_{sp}}{A_{\rm eff}^2}\,\delta A_{\rm eff}\,dz,$$

where the left-hand sides (LHSs) are obtained after integrating by parts, and we have introduced

$$Q_{uv} = \beta(P_u^+ + 2P_u^-) + \zeta_{uv}(P_v^+ + P_v^-) + 2\kappa_u\frac{\mathcal{P}^2}{A_{\rm eff}}.$$

Adding these equations termwise and utilizing the boundary conditions

$$\delta P_p^+(0) = R_{p0}\delta P_p^-(0), \quad \text{(A2a)}$$

$$\delta P_s^+(0) = R_{s0}\delta P_s^-(0), \quad \text{(A2b)}$$

$$\delta P_p^-(L) = R_{pL}\delta P_p^+(L), \quad \text{(A2c)}$$

$$\delta P_s^-(L) = R_{sL}\delta P_s^+(L) = 0, \quad \text{(A2d)}$$

which follow from (2), we can represent the LHS of the resulting equation in the form

$$\begin{aligned}\text{LHS} = {} & [\varphi_+(L) + R_{pL}\varphi_-(L)]\,\delta P_p^+(L) \\ & - [\varphi_-(0) + R_{p0}\varphi_+(0)]\,\delta P_p^-(0) \\ & - [\psi_-(0) + R_{s0}\psi_+(0)]\,\delta P_s^-(0) \\ & - \int_0^L\left(\delta P_p^+\frac{d\varphi_+}{dz} + \delta P_p^-\frac{d\varphi_-}{dz} + \delta P_s^+\frac{d\psi_+}{dz} + \delta P_s^-\frac{d\psi_-}{dz}\right)dz.\end{aligned}$$

If now we impose on auxiliary functions the conditions (7), only the integral term survives in this expression. The right-hand side (RHS) of the resulting equation is given by

$$\begin{aligned}\text{RHS} = {} & -\int_0^L \big[(a_p^+\varphi_+ - \widetilde{a}_p^+\varphi_- + b_p^+\psi_+ - \widetilde{b}_p^+\psi_-)\,\delta P_p^+ \\ & + (a_p^-\varphi_+ - \widetilde{a}_p^-\varphi_- + b_p^-\psi_+ - \widetilde{b}_p^-\psi_-)\,\delta P_p^- \\ & + (b_s^+\varphi_+ - \widetilde{b}_s^+\varphi_- + a_s^+\psi_+ - \widetilde{a}_s^+\psi_-)\,\delta P_s^+ \\ & + (b_s^-\varphi_+ - \widetilde{b}_s^-\varphi_- + a_s^-\psi_+ - \widetilde{a}_s^-\psi_-)\,\delta P_s^-\big]dz \\ & + \int_0^L \frac{\delta A_{\rm eff}}{A_{\rm eff}^2}\big\{\varphi_+ P_p^+[\beta(P_p^+ + 2P_p^-) + \zeta_{ps}(P_s^+ + P_s^-)] \\ & - \varphi_- P_p^-[\beta(P_p^- + 2P_p^+) + \zeta_{ps}(P_s^+ + P_s^-)] \\ & + \psi_+ P_s^+[\beta(P_s^+ + 2P_s^-) + \zeta_{sp}(P_p^+ + P_p^-)] \\ & - \psi_- P_s^-[\beta(P_s^- + 2P_s^+) + \zeta_{sp}(P_p^+ + P_p^-)]\big\}dz\end{aligned}$$

$$+\int_0^L \frac{\delta A_{\text{eff}}}{A_{\text{eff}}^3}\, 2\mathcal{P}^2 \left[\kappa_p(\varphi_+ P_p^+ - \varphi_- P_p^-) + \kappa_s(\psi_+ P_s^+ - \psi_- P_s^-)\right] dz.$$

The comparison of LHS and RHS with the corresponding parts of (A1) shows that $A_{\text{eff}}(z)$ is given by (5), if (6) and conditions given in (7) are satisfied.

REFERENCES

[1] B. Jalali, S. Yegnanarayanan, T. Yoon, T. Yoshimoto, I. Rendina, and F. Coppinger, "Advances in silicon-on-insulator optoelectronics," *IEEE J. Sel. Top. Quantum Electron.*, vol. 4, no. 6, pp. 938–947, Nov./Dec. 1998.

[2] B. Jalali, O. Boyraz, V. Raghunathan, D. Dimitropoulos, and P. Koonath, "Silicon Raman amplifiers, lasers and their applications," in *Proc. SPIE Active Passive Opt. Componen. WDM Commun. V*, vol. 6014, pp. 21–26, 2005.

[3] R. A. Soref, "The past, present, and future of silicon photonics," *IEEE J. Sel. Top. Quantum Electron.*, vol. 12, no. 6, pp. 1678–1687, Nov./Dec. 2006.

[4] H. K. Tsang and Y. Liu, "Nonlinear optical properties of silicon waveguides," *Semicond. Sci. Technol.*, vol. 23, pp. 064007-1–064007-9, 2008.

[5] Q. Lin, O. J. Painter, and G. P. Agrawal, "Nonlinear optical phenomena in silicon waveguides: Modeling and applications," *Opt. Exp.*, vol. 15, pp. 16604–16644, 2007.

[6] D. Dimitropoulos, B. Houshmand, R. Claps, and B. Jalali, "Coupled-mode theory of Raman effect in silicon-on-insulator waveguides," *Opt. Lett.*, vol. 28, pp. 1954–1956, 2003.

[7] B. Jalali, V. Raghunathan, D. Dimitropoulos, and O. Boyraz, "Raman-based silicon photonics," *IEEE J. Sel. Top. Quantum Electron.*, vol. 12, no. 3, pp. 412–421, May/Jun. 2006.

[8] R. Claps, D. Dimitropoulos, V. Raghunathan, Y. Han, and B. Jalali, "Observation of stimulated Raman amplification in silicon waveguides," *Opt. Exp.*, vol. 11, pp. 1731–1739, 2003.

[9] R. Claps, D. Dimitropoulos, and B. Jalali, "Stimulated Raman scattering in silicon waveguides," *Electron. Lett.*, vol. 38, no. 22, pp. 1352–1354, Oct. 2002.

[10] G. P. Agrawal, *Nonlinear Fiber Optics*. Boston, MA: Academic, 2007.

[11] X. Chen, N. C. Panoiu, and R. M. Osgood, "Theory of Raman-mediated pulsed amplification in silicon-wire waveguides," *IEEE J. Quantum Electron.*, vol. 42, no. 2, pp. 160–170, Feb. 2006.

[12] A. Liu, H. Rong, M. Paniccia, O. Cohen, and D. Hak, "Net optical gain in a low loss silicon-on-insulator waveguide by stimulated Raman scattering," *Opt. Exp.*, vol. 12, pp. 4261–4268, 2004.

[13] T. K. Liang and H. K. Tsang, "Efficient Raman amplification in silicon-on-insulator waveguides," *Appl. Phys. Lett.*, vol. 85, pp. 3343–3356, 2004.

[14] Q. Xu, V. Almeida, and M. Lipson, "Time-resolved study of Raman gain in highly confined silicon-on-insulator waveguides," *Opt. Exp.*, vol. 12, pp. 4437–4442, 2004.

[15] O. Boyraz and B. Jalali, "Demonstration of 11 dB fiber-to-fiber gain in a silicon Raman amplifier," *IEICE Electron. Exp.*, vol. 1, pp. 429–434, 2004.

[16] R. Espinola, J. Dadap, R. Osgood, S. J. McNab, and Y. A. Vlasov, "Raman amplification in ultrasmall silicon-on-insulator wire waveguides," *Opt. Exp.*, vol. 12, pp. 3713–3718, 2004.

[17] R. Jones, H. Rong, A. Liu, A. W. Fang, M. J. Paniccia, D. Hak, and O. Cohen, "Net continuous-wave optical gain in a low loss silicon-on-insulator waveguide by stimulated Raman scattering," *Opt. Exp.*, vol. 13, pp. 519–525, 2005.

[18] M. Krause, H. Renner, S. Fathpour, B. Jalali, and E. Brinkmeyer, "Gain enhancement in cladding-pumped silicon Raman amplifiers," *IEEE J. Quantum Electron.*, vol. 44, no. 7, pp. 692–704, Jul. 2008.

[19] S. Roy, S. K. Bhadra, and G. P. Agrawal, "Raman amplification of optical pulses in silicon waveguides: effects of finite gain bandwidth, pulse width, and chirp," *J. Opt. Soc. Amer. B*, vol. 26, pp. 17–25, 2009.

[20] R. Claps, V. Raghunathan, D. Dimitropoulos, and B. Jalali, "Influence of nonlinear absorption on Raman amplification in Silicon waveguides," *Opt. Exp.*, vol. 12, pp. 2774–2780, 2004.

[21] T. K. Liang and H. K. Tsang, "Nonlinear absorption and Raman scattering in silicon-on-insulator optical waveguides," *IEEE J. Sel. Top. Quantum Electron.*, vol. 10, no. 5, pp. 1149–1153, Sep./Oct. 2004.

[22] T. K. Liang and H. K. Tsang, "Role of free carriers from two-photon absorption in Raman amplification in silicon-on-insulator waveguides," *Appl. Phys. Lett.*, vol. 84, pp. 2745–2747, 2004.

[23] D. Dimitropoulos, R. Jhaveri, R. Claps, J. C. S. Woo, and B. Jalali, "Lifetime of photogenerated carriers in silicon-on-insulator rib waveguides," *Appl. Phys. Lett.*, vol. 86, pp. 071115-1–071115-3, 2005.

[24] S. Fathpour, K. K. Tsia, and B. Jalali, "Energy harvesting in silicon Raman amplifiers," *Appl. Phys. Lett.*, vol. 89, pp. 061109-1–061109-3, 2006.

[25] A. Liu, H. Rong, R. Jones, O. Cohen, D. Hak, and M. Paniccia, "Optical amplification and lasing by stimulated Raman scattering in silicon waveguides," *J. Lightwave Technol.*, vol. 24, no. 3, pp. 1440–1455, Mar. 2006.

[26] H. Renner, M. Krause, and E. Brinkmeyer, "Maximal gain and optimal taper design for Raman amplifiers in silicon-on-insulator waveguides," presented at the Integr. Photon. Res. Appl. Top. Meetings, (IPRA 2005), San Diego, CA, paper JWA3.

[27] M. Krause, H. Renner, and E. Brinkmeyer, "Efficiency increase of silicon-on-insulator Raman lasers by reduction of free-carrier absorption in tapered waveguides," in *Proc. Conf. Lasers Electro-Opt.,* (CLEO 2005), paper CThB1, pp. 1548–1550.

[28] M. Krause, H. Renner, and E. Brinkmeyer, "Efficient Raman lasing in tapered silicon waveguides," *Spectroscopy*, vol. 21, pp. 26–32, 2006.

[29] I. D. Rukhlenko, M. Premaratne, C. Dissanayake, and G. P. Agrawal, "Maximization of net optical gain in silicon-waveguide Raman amplifiers," *Opt. Exp.*, vol. 17, pp. 5807–5814, 2009.

[30] M. Krause, H. Renner, and E. Brinkmeyer, "Analysis of Raman lasing characteristics in silicon-on-insulator waveguides," *Opt. Exp.*, vol. 12, pp. 5703–5710, 2004.

[31] C. Fox, *An Introduction to the Calculus of Variations*. New York: Dover, 1987.

Ivan D. Rukhlenko received the B.Sc. (phys.) and M.Sc. (phys.) degrees with honors from the Saint-Petersburg State Technical University, Saint-Petersburg, Russia, in 2001 and 2003, respectively, and the Ph.D. degree in optics from the Saint-Petersburg State University of Informational Technologies, Mechanics and Optics, Saint-Petersburg, in 2006.

From 2006 to 2008, he was a Research Fellow with the Department of Optics of Nanostructures, Center of Informational Optical Technologies, Saint-Petersburg State University of Informational Technologies, Mechanics and Optics. He is currently a Research Fellow with the Advanced Computing and Simulation Laboratory, Department of Electrical and Computer Systems Engineering, Monash University, Clayton, Vic., Australia. He is the author of more than 10 research papers in the area of physics of low-dimensional structures. His research interests include nonlinear effects in silicon photonics, dynamics of spectroscopic transitions in quantum dots, quantum dot secondary emission, and propagation of elementary excitations in semiconductor heterostructures.

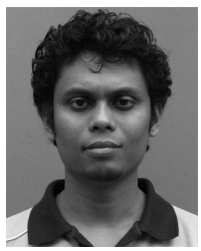

Chethiya Dissanayake received the B.Sc. (Eng.) degree in electronics and telecommunication engineering with a first class honors from the University of Moratuwa, Katubedda, Sri Lanka, in 2005. He is currently working toward the M.Sc. degree in silicon photonics at the Advanced Computing and Simulation Laboratory, Monash University, Clayton, Vic., Australia.

Fom 2005 to 2007, he was a Telecommunication Engineer with the Research and Development Laboratory, Electroteks Global Networks (Pte.) Ltd., Ratmalana, Sri Lanka. His current research interests include silicon photonics, silicon Raman amplifiers with emphasis on numerical modeling.

Malin Premaratne (S'95–M'98–SM'03) received the B.Sc. (maths.) and B.E. (elec.) degrees with first class honors, and the Ph.D. degree from the University of Melbourne, Melbourne, Vic., Australia, in 1995, and 1998, respectively.

From 1998 to 2000, he was with the Photonics Research Laboratory, a division of Australian Photonics Cooperative Research Center (APCRC), University of Melbourne, where he was the Coproject Leader of the APCRC Optical Amplifier Project. During this period, he was engaged with Telstra, Melbourne, Vic., and Hewlett Packard, Palo Alto, CA, through the University of Melbourne. From 2000 to 2003, he was involved with several leading startups in the photonic area either as an Employee or a Consultant. During this period, he has also served in the editorial boards of SPIE/Kluwer and Wiley publishers in the optical communications area. From 2001 to 2003, he was a Product Manger (Research and Development) with VPI Systems Optical Systems Group, Holmdel, NJ. He has been steering the research program in high-performance computing applications to complex systems simulations with the Advanced Computing and Simulation Laboratory, Monash University, Clayton, Vic., since 2003, where he is currently the Research Director and an Associate Professor. He is the author of more than 100 research papers in the areas of semiconductor lasers, erbium-doped fiber amplifier and Raman amplifiers, optical network design algorithms, and numerical simulation techniques. Currently, he also holds visiting research appointments with The University of Melbourne, Australian National University, Canberra, University of California, Los Angeles, and University of Rochester, Rochester, NY.

Dr. Premaratne is a Fellow and an Executive Member of the Institution of Engineers Australia, Melbourne, Vic. He has been serving as the Chairman of IEEE Lasers and Electro-Optics Society, Melbourne, Vic., since 2001.

Govind P. Agrawal (M'83–SM'86–F'96) received the B.Sc. degree from the University of Lucknow, Lucknow, India, in 1969, and the M.Sc. and Ph.D. degrees from the Indian Institute of Technology, New Delhi, in 1971 and 1974, respectively.

He was with the Ecole Polytechnique, Lyon, France, City University of New York, New York, NY, and AT&T Bell Laboratories, Murray Hill, NJ. He has been with the Institute of Optics, University of Rochester, Rochester, NY, since 1989, where he is currently a Professor of optics. His research interests include optical communications, nonlinear optics, and laser physics. He is the author or coauthor of more than 300 research papers, several book chapters and review articles, and seven books, e.g., *Semiconductor Laser* (Norwell, MA: Kluwer Academic, 2nd ed., 1993); *Fiber-Optic Communication Systems* (Hoboken, NJ: Wiley, 3rd ed., 2002); *Nonlinear Fiber Optics* (Boston: Academic Press, 4th ed., 2007); *Applications of Nonlinear Fiber Optics* (Boston: Academic Press, 2nd ed., 2008); *Optical Solutions: From Fibers to Photonic Crystals* (San Diego, CA: Academic Press, 2003); *Lightwave Technology: Components and Devices* (Hoboken, NJ: Wiley, 2004); and *Lightwave Technology: Telecommunication System* (Hoboken, NJ: Wiley, 2005).

Dr. Agrawal is a Fellow of the Optical society of America (OSA). He is also a Life Fellow of the Optical Society of India. He has participated multiple times in organizing technical conferences sponsored by IEEE and OSA. He was the General Cochair in 2001 for the Quantum Electronics and Laser Science Conference and a Member of the Program committee for the Conference on Lasers and Electro-Optic in 2004 and 2005, respectively.